














Integrating GWAS and TWAS to elucidate the genetic architecture of maize leaf cuticular conductance

Meng Lin ¹, Pengfei Qiao ², Susanne Matschi ^{3,†}, Miguel Vasquez ³,
Guillaume P. Ramstein ^{4,‡}, Richard Bourgault ⁵, Marc Mohammadi ⁵, Michael J. Scanlon ²,
Isabel Molina ⁵, Laurie G. Smith ³ and Michael A. Gore ^{1,*,#}

- 1 Plant Breeding and Genetics Section, School of Integrative Plant Science, Cornell University, Ithaca, New York 14853, USA
- 2 Plant Biology Section, School of Integrative Plant Science, Cornell University, Ithaca, New York 14853, USA
- 3 Section of Cell and Developmental Biology, University of California San Diego, La Jolla, California 92093, USA
- 4 Institute for Genomic Diversity, Cornell University, Ithaca, New York 14853, USA
- 5 Department of Biology, Algoma University, Sault Ste Marie, ON P6A 2G4, Canada

*Author for correspondence: mag87@cornell.edu

†Present address: Leibniz Institute of Plant Biochemistry, Halle (Saale), 06120, Germany.

‡Present address: Center for Quantitative Genetics and Genomics, Aarhus University, Aarhus, 8000, Denmark.

#Senior author

M.A.G., L.G.S., M.J.S., and I.M. conceived the research plans and supervised the experiments. S.M. and M.V. managed fields, collected tissue samples, and generated and analyzed data for cuticular conductance and guard cell structural features; R.B. and M.M. performed cuticular wax analysis. P.Q. performed 3' mRNA-seq data analysis. G.P.R. provided technical assistance to M.L. for genotype imputation. M.L. performed most of the data analysis and wrote the article with contributions of all the authors. M.A.G. agrees to serve as the author responsible for contact and ensures communication.

The author responsible for distribution of materials integral to the findings presented in this article in accordance with the policy described in the Instructions for Authors (<https://academic.oup.com/plphys/pages/general-instructions>) is Michael A. Gore (mag87@cornell.edu).

Abstract

The cuticle, a hydrophobic layer of cutin and waxes synthesized by plant epidermal cells, is the major barrier to water loss when stomata are closed. Dissecting the genetic architecture of natural variation for maize (*Zea mays* L.) leaf cuticular conductance (g_c) is important for identifying genes relevant to improving crop productivity in drought-prone environments. To this end, we performed an integrated genome- and transcriptome-wide association studies (GWAS and TWAS) to identify candidate genes putatively regulating variation in leaf g_c . Of the 22 plausible candidate genes identified, 4 were predicted to be involved in cuticle precursor biosynthesis and export, 2 in cell wall modification, 9 in intracellular membrane trafficking, and 7 in the regulation of cuticle development. A gene encoding an INCREASED SALT TOLERANCE1-LIKE1 (*ISTL1*) protein putatively involved in intracellular protein and membrane trafficking was identified in GWAS and TWAS as the strongest candidate causal gene. A set of maize nested near-isogenic lines that harbor the *ISTL1* genomic region from eight donor parents were evaluated for g_c , confirming the association between g_c and *ISTL1* in a haplotype-based association analysis. The findings of this study provide insights into the role of regulatory variation in the development of the maize leaf cuticle and will ultimately assist breeders to develop drought-tolerant maize for target environments.

Introduction

The cuticle is a hydrophobic layer covering the epidermal surfaces of the shoot, which protects plants from dehydration, UV radiation, and pathogen attack (Shepherd and Wynne Griffiths, 2006; Xue et al., 2017). Cutin and waxes are the two major lipid components comprising the plant cuticle. Cutin is an insoluble matrix formed by extensive ester cross-linking of fatty acid derivatives and glycerol (Pollard et al., 2008; Fich et al., 2016). Soluble waxes, including alkanes, aldehydes, alcohols, ketones, and wax esters, are embedded within and on top of the cutin matrix (Yeats and Rose, 2013).

Cuticle composition and structure influence its water barrier function (Kerstiens, 2006). However, cuticle impermeability to water is not simply determined by wax load or cuticle thickness; instead, chemical composition and the organization of cuticle components appear to contribute to reducing nonstomatal water loss (Riederer and Schreiber, 2001). Thus, cuticle composition and structure are potentially relevant to plant drought tolerance. Mutants and transgenic plants with reduced wax load and compromised cuticle structure often show increased cuticular permeability and decreased drought tolerance (Zhou et al., 2013; Zhu and Xiong, 2013; Li et al., 2019), while overexpression of cuticle lipid biosynthesis enzymes or their transcriptional regulators can result in increased cuticular lipid abundance and drought tolerance (Aharoni et al., 2004; Zhang et al., 2005; Bourdenx et al., 2011; Wang et al., 2012). In wheat (*Triticum aestivum* L.) and barley (*Hordeum vulgare* L.), glaucousness, a visual manifestation of epicuticular wax crystals, was selected for during domestication (Bi et al., 2016; Hen-Avivi et al., 2016) and shows positive associations with drought tolerance (Febrero et al., 1998; Guo et al., 2016; Busta et al., 2021). Collectively, these findings suggest a range of possibilities toward increased drought tolerance via cuticle modification in cereal crops.

Biological pathways involved in cuticle development affect its permeability to water in different ways. The formation of the plant cuticle requires not only the synthesis of cutin monomers and cuticular waxes but also the transport and polymerization of cutin monomers after transport (Yeats and Rose, 2013). Major pathways for the biosynthesis of cutin monomers and cuticular waxes have been elucidated in model plant systems (Yeats and Rose, 2013; Lee and Suh, 2015; Fich et al., 2016). A Golgi-mediated vesicle trafficking system delivers cuticle lipids from the intracellular membranes, where they are synthesized, to the plasma membrane (McFarlane et al., 2014) for export by ATP-BINDING CASSETTE TRANSPORTER G (ABCG) family proteins (Pighin et al., 2004; Bird et al., 2007; Panikashvili et al., 2010; Bessire et al., 2011; Chen et al., 2011) and extracellular lipid transport proteins (DeBono et al., 2009; Kim et al., 2012). In addition, GLY-ASP-SER-LEU ESTERASE/LIPASE (GDSL lipase) is required for cutin polymerization in the developing cuticle (Girard et al., 2012; Yeats and Rose, 2013), and the degree of pectin esterification is critical to cuticle structure by facilitating the diffusion of cutin precursors (Bakan and Marion,

2017; Philippe et al., 2020). Transcription factors have also been identified to regulate various steps in cuticle development (Borisjuk et al., 2014; Elango et al., 2020), but how these transcription factors, biosynthesis, and transport processes work together is not well understood.

Genome-wide association studies (GWAS) are widely used to identify genomic variants associated with a trait of interest (Tibbs Cortes et al., 2021). As in a prior study (Lin et al., 2020), this study uses GWAS to investigate cuticular conductance (g_c) in adult maize (*Zea mays* L.) leaves defined as the rate of water loss from detached leaves when stomata are closed, an indirect measure of cuticle permeability to water. The dark treatment used was more than sufficient to close stomata in a variety of tested genotypes (Lin et al., 2020), but leakage of water vapor through closed stomata could contribute to rates of water loss in our g_c assay. Nevertheless, several *Arabidopsis* (*Arabidopsis thaliana*) mutants with biochemically characterized cuticular wax abnormalities show increased rates of shoot tissue dehydration in assays similar to ours, and also have increased cuticular permeance as measured by more direct methods (Chen et al., 2003; Aharoni et al., 2004; Sadler et al., 2016). Moreover, unlike these more direct methods (reviewed in Valeska Zeisler-Diehl et al., 2017), the methodology we used is scalable to achieve the throughput needed for GWAS. Our prior GWAS (Lin et al., 2020) demonstrated that g_c in adult maize leaves is likely controlled by large numbers of small effect alleles in maize, which agrees with the complex cuticle biosynthesis network and transport mechanisms (Yeats and Rose 2013).

Transcriptome-wide association studies (TWAS), which identify significant associations between trait variation and transcript abundances across all expressed genes in a tissue, can provide complementary information for candidate gene identification in an independent test. Furthermore, integrating GWAS and TWAS results with an ensemble approach based on the Fisher's combined test (FCT) improves statistical power in candidate gene identification (Kremling et al., 2019), especially for leaf physiological traits with a complex genetic architecture (Ferguson et al., 2021; Pignon et al., 2021). Thus, in this study, we sought to bypass limitations of our earlier GWAS by using an expanded set of ~9 million single nucleotide polymorphism (SNP) markers for GWAS, and by combining results of GWAS and TWAS via FCT to achieve gene-level resolution of candidate regulators of g_c . Evaluation of maize nested near-isogenic lines (nNILs) (Morales et al., 2020) confirmed the association between g_c and one of the identified plausible causal genes, which encodes a predicted INCREASED SALT TOLERANCE1-LIKE1 (ISTL1) protein.

Results

Relationship of g_c to cuticle composition and structure

Permeability of the leaf cuticle to water was measured as g_c on 310 genetically representative maize inbred lines [89 lines

showing the highest or lowest g_c in Lin et al. (2020) and 234 lines representing the maximal genetic diversity] from the Wisconsin Diversity (WiDiv) panel that were evaluated in two environments in San Diego, CA. To investigate how this phenotype of moderately high heritability ($\hat{h}_1^2 = 0.73$) related to cuticle characteristics, we quantitatively analyzed selected features of adult leaf cuticle composition and structure in a subset of 51 WiDiv lines with highest and lowest g_c values. Our structural analysis focused on features of guard cell cuticles that could be analyzed quantitatively in a large number of samples via confocal microscopy and seemed likely to affect the g_c trait. As illustrated in Supplemental Figure S1, we observed cuticular flaps projecting from the inner surfaces of guard cell pores, as described in many plant species, often called “outer cuticular ledges” (e.g. Hunt et al., 2017), which have been proposed to reduce water loss by enhancing the seal of closed stomata (Wilmer and Fricker, 1996; Zhao and Sack, 1999; Kosma and Jenks, 2007). We also observed cuticular bumps lining stomatal pores, which appear to permit a “zippering” of closed stomata (Supplemental Figure S1). However, variation in these traits was only weakly associated with g_c ($|r| < 0.12$ for all measures; Supplemental Table S1). Numerous studies have demonstrated relationships between cuticular wax composition and cuticle permeability (Zhou et al., 2013; Zhu and Xiong, 2013; Li et al., 2019), and wax composition was also found to vary in these extreme g_c lines. Therefore, we also investigated how variation in g_c may be related to wax composition. Significant associations ($P < 0.05$) were observed between g_c and a subset of fatty acids, wax esters, aldehydes, and alicyclics ($r = -0.290$ to -0.488 ; Supplemental Table S1).

To further query the relationship of g_c to cuticular wax composition and structural features, random forest analysis was conducted with five-fold cross-validation to determine the degree to which g_c can be predicted by the analyzed features, and which features are the strongest drivers of predictive ability. As shown in Figure 1 and Supplemental Table S1, we found that the abundance of several long chain wax esters and aldehydes (especially C54 wax esters and C30 aldehydes) to be important predictors of g_c . The overall predictive ability for g_c from all measured characteristics combined was 0.35, with most of the predictive power coming from measurements of C54 wax esters and C30 aldehydes. The relationship of g_c to C54 wax ester abundance is interesting in relation to the findings of Bourgault et al. (2020), showing that acquisition of mature water barrier function during cuticle development in adult maize leaves coincided with a shift from alkanes to esters with carbon chain lengths more than 49 as the most abundant wax class. Thus, our analysis of wax composition in extreme lines provides further evidence of a role for wax esters in protecting adult maize leaves against water loss, consistent with recent findings in Arabidopsis (Patwari et al., 2019). However, the majority of g_c is not explained by the cuticle features we analyzed, underscoring the complexity of this trait that

merits further genetic examination through the combination of GWAS and TWAS.

Quantitative genetic analysis for identification of candidate genes for g_c

To improve statistical power in the identification of candidate genes for g_c beyond that achieved in GWAS alone by Lin et al. (2020), we performed the FCT to integrate GWAS and TWAS results (see “Materials and methods” for more details). A total of 319 candidates (top 1%) were identified from FCT (Supplemental Table S2), 273 (top 0.01%) from GWAS (Supplemental Tables S3 and S4), and 200 (top 1%) from TWAS (Supplemental Table S5). Five genes were identified by GWAS and TWAS (*Zm00001d049479*, *Zm00001d038819*, *Zm00001d039391*, *Zm00001d049174*, and *Zm00001d053966*) and four of these (all but *Zm00001d053966*) were identified by all three methods. However, only one of these, *Zm00001d049479* (ISTL1, discussed below), has a predicted function plausibly related to cuticles. Considering all candidate genes listed in Supplemental Tables S2, S4, and Table S5, a total of 22 such plausible candidates were selected based on predicted functions and were assigned to one of four functional categories (Table 1; Supplemental Figure S2). Fourteen of these plausible candidates were identified by FCT, five by TWAS, and three by GWAS; nine were identified by two or more of these strategies. Supplemental Table S6 lists the closest Arabidopsis and rice relatives of these 22 genes.

Of the 14 plausible candidate genes identified by FCT, one (*Zm00001d049479*) encoding the closest maize relative of ISTL1 in Arabidopsis, which functions in multivesicular body formation within endosomes (Buono et al., 2016), was also identified by both TWAS and GWAS (Table 1; Figure 2). Additionally, 5 of the 14 genes identified by FCT encode proteins with predicted functions in intracellular membrane trafficking, 3 of which were also identified by TWAS (Table 1). Two of these five, *Zm00001d039411* and *Zm00001d012964*, encode proteins with sequence identity to $\alpha 1$ COAT PROTEIN ($\alpha 1$ -COP) and SECRETION 14 (SEC14) in Arabidopsis, respectively, which function in vesicle formation at the Golgi surface (Jouannic et al., 1998; Lee and Goldberg, 2010). *Zm00001d051599* and *Zm00001d025180* encode proteins with Rab GTPase-activating protein (Rab-GAP) domains, predicted to function in regulation of vesicle transport (Stenmark, 2009), and *Zm00001d022364* encodes a soluble NSF attachment protein receptor (SNARE) homolog with an expected function in vesicle fusion with target membranes (Chen and Scheller, 2001).

The remaining eight plausible candidate genes identified by FCT, four of which were also identified by TWAS and one also by GWAS, encode proteins with a variety of functions. Two (*Zm00001d048953* and *Zm00001d015477*, 3-KETOACYL-COA SYNTHASE 3 [KCS3], and GLOSSY1-like/ECERIFERUM3-like [GL1-like/CER3-like], respectively), are homologs of Arabidopsis genes with functions in cuticular

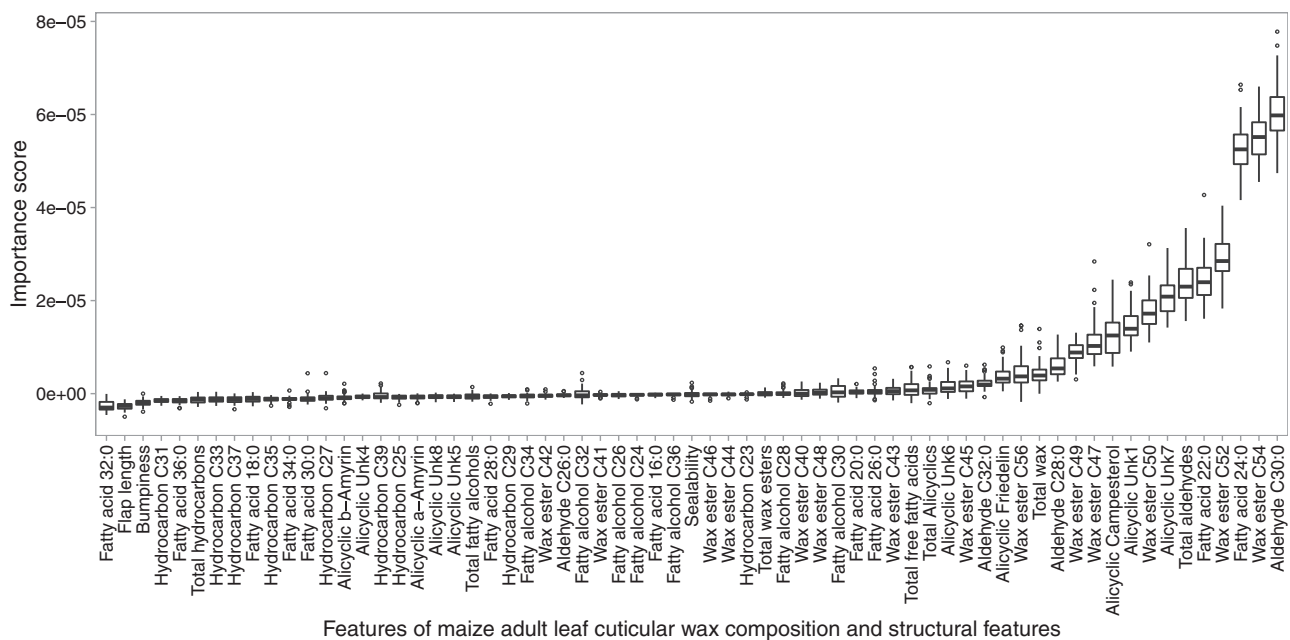


Figure 1 Box plot of importance scores for cuticular wax composition and structural features in random forest regression to predict maize g_c using five-fold cross validation 50 times. Box limits indicate the upper and lower quartiles; center lines in boxes indicate the median value; whiskers indicate $1.5 \times$ interquartile range; and dots indicate outliers.

Table 1 Plausible candidate genes identified in a genome-wide association study (GWAS), a transcriptome-wide association study (TWAS), and the Fisher's combined test (FCT) for g_c in the WiDiv panel

Gene ID	Annotation	Chromosome	Gene Start	Gene End	Functional Category ^b	Method
Zm00001d029141	MIEL1-like	1	60,322,950	60,326,019	RCD	GWAS, FCT
Zm00001d032788	GDSL esterase/lipase	1	238,190,770	238,192,464	CBE	TWAS, FCT
Zm00001d002843	MYB54	2	24,293,846	24,295,521	RCD	FCT
Zm00001d005087	GLK35	2	157,736,007	157,737,776	RCD	TWAS, FCT
Zm00001d039411	α 1-COP	3	3,708,911	3,716,373	IMT	TWAS, FCT
Zm00001d040788	SEC15B	3	65,988,895	65,991,327	IMT	GWAS
Zm00001d042612	CER7	3	173,571,381	173,573,177	RCD	FCT
Zm00001d043509	PME40	3	202,333,699	202,335,784	CWB	TWAS
Zm00001d044162	WRKY64	3	220,824,499	220,827,409	RCD	TWAS
Zm00001d048953	KCS3	4	10,603,315	10,607,553	CBE	TWAS, FCT
Zm00001d049479	ISTL1	4	31,729,260	31,732,664	IMT	GWAS, TWAS, FCT
Zm00001d050185	MYB108	4	71,478,007	71,479,474	RCD	TWAS
Zm00001d051599	Rab-GAP/TBC	4	164,071,426	164,090,678	IMT	TWAS, FCT
Zm00001d012964	SEC14	5	2,431,015	2,437,696	IMT	FCT
Zm00001d015477	CER3-like	5	92,669,605	92,675,745	CBE	TWAS, FCT
Zm00001d036765	CER9	6	100,099,887	100,107,565	RCD	TWAS
Zm00001d038404/ Zm00001d038405 ^a	Ypt/Rab-GAP	6	156,394,901/ 156,409,880	156,403,240/ 156,412,505	IMT	GWAS
Zm00001d022364	SNARE	7	176,149,978	176,160,500	IMT	TWAS, FCT
Zm00001d010426	CER5/ABCG12-like	8	114,527,255	114,533,597	CBE	TWAS
Zm00001d012175	PAE5	8	169,547,499	169,551,527	CWB	FCT
Zm00001d025180	Ypt/Rab-GAP	10	107,999,211	108,003,428	IMT	FCT

^aIn B73 RefGen_v4, this gene was erroneously split into the two gene models as indicated, but in B73 RefGen_v5 they have been correctly merged into a single gene model with identifier Zm00001eb289920.

^bRCD, regulator of cuticle development; CBE, cuticle biosynthesis and export; IMT, intracellular membrane trafficking; CWB, cell wall biosynthesis.

wax biosynthesis (Lee et al., 2009; Bernard et al., 2012). A third (Zm00001d032788) encodes a predicted GDSL esterase/lipase gene closely related to Arabidopsis and tomato (*Solanum lycopersicum* L.) cutin synthases (Girard et al., 2012; Yeats et al., 2012). Two FCT-identified genes [Zm00001d005087 and Zm00001d002843, annotated as G2-

LIKE-TRANSCRIPTION FACTOR 35 (GLK35) and MYB54, respectively), encode transcription factors with potential functions in regulation of cuticle biosynthesis (Kant et al., 2008; Dubos et al., 2010; Oshima and Mitsuda, 2013). Zm00001d029141 is a homolog of Arabidopsis MYB30-INTERACTING E3 LIGASE 1 (MIEL1), which regulates the

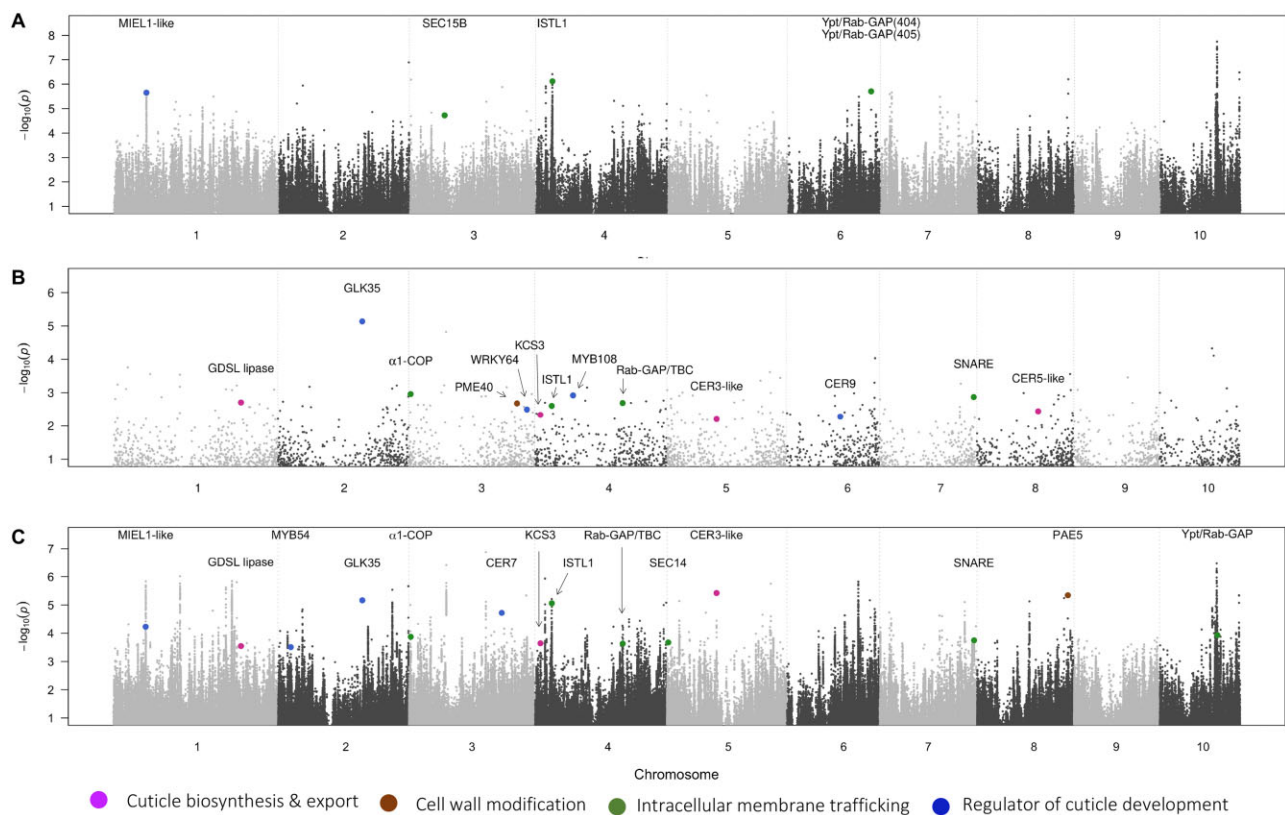


Figure 2 Manhattan plot of results from an integrated quantitative genetic analysis of adult maize g_c across two environments in San Diego, CA. A, Genome-wide association study: the $-\log_{10} P$ -value of each SNP tested in a mixed linear model analysis of g_c is plotted as a point against its physical position (B73 RefGen_v4) for the 10 chromosomes of maize. The peak SNPs closest to plausible candidate genes are colored based on their functional categories. B, Transcriptome-wide association study: the $-\log_{10} P$ -value of each gene transcript tested in a mixed linear model analysis of g_c is plotted as a point against its physical position (B73 RefGen_v4). Plausible candidate genes are colored based on their functional categories. C, Fisher's combined test (FCT): the $-\log_{10} P$ -value of each of the top 10% SNPs in GWAS paired with the nearest gene in FCT plotted as a point against its physical position (B73 RefGen_v4). The top 1% of SNP gene pairs related to plausible candidate genes identified in the FCT are colored based on their functional categories.

stability of two MYB family regulators of wax biosynthesis (Marino et al., 2013; Gil et al., 2017). *Zm00001d042612* encodes a homolog of Arabidopsis CER7, a core subunit of the RNA degrading exosome associated with alkane biosynthesis (Hooker et al., 2007). The final FCT-identified gene listed in Table 1, *Zm00001d012175* (PECTIN ACETYLESTERASE 5 [PAE5]), encodes a predicted pectin-modifying enzyme.

A total of five additional plausible candidate genes were uniquely detected by TWAS (Figure 2; Table 1). *Zm00001d043509* encodes a PECTIN METHYLESTERASE 40 (PME40). *Zm00001d010426* encodes a homolog of Arabidopsis CER5/ABCG12, which functions in cuticular wax secretion (Pighin et al., 2004). *Zm00001d036765* encodes a homolog of Arabidopsis CER9, which regulates the abundance of both cutin and cuticular waxes (Lü et al., 2012). The two remaining TWAS-identified genes (*Zm00001d050185* and *Zm00001d044162*) encode homologs of Arabidopsis WRKY and MYB family transcription factors with potential roles in cuticle development, which are differentially expressed across maize leaf cuticular developmental stages (Qiao et al., 2020).

GWAS uniquely identified three additional plausible candidate genes predicted to be involved in the intracellular

membrane trafficking system (Figure 2; Table 1). Two adjacent genes (*Zm00001d038404* and *Zm00001d038405*) putatively encode Ypt/Rab-GAPs, regulators of vesicle fusion (Stenmark, 2009). *Zm00001d040788* encodes a homolog of Arabidopsis SEC15B, an exocyst subunit that activates vesicle fusion with the plasma membrane during polarized secretion (Guo et al., 1999; Mayers et al., 2017).

Haplotype-based association analysis for g_c in the WiDiv panel

The *ISTL1* gene emerged from our analysis as a strong candidate regulator of g_c since it was identified in our prior GWAS (Lin et al., 2020) and the only gene detected by all three analyses (GWAS, TWAS, and FCT) in this study. To further investigate the association between g_c and genetic variation within the WiDiv population in the vicinity of *ISTL1*, we analyzed the association between g_c and haplotypes at 91 haploblocks (blocks of haplotypes) within 200 kb of *ISTL1*. Of these, Block 65 was the most significantly associated with g_c ($P = 4.07 \times 10^{-7}$) in the WiDiv panel (Figure 3; Supplemental Table S7), having three haplotypes defined by three SNPs including the peak GWAS SNP

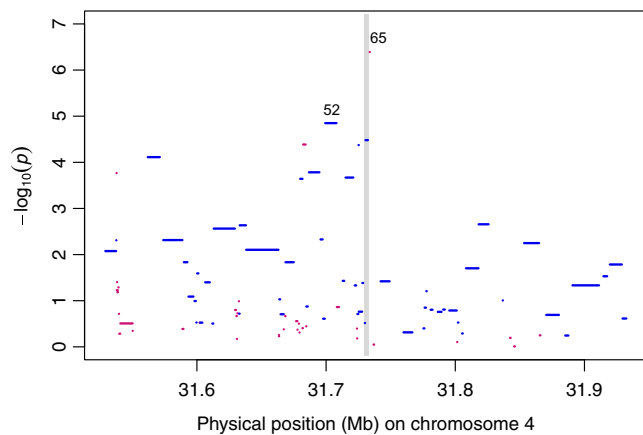


Figure 3 Manhattan plot of results from a haplotype-based association analysis in the vicinity of *ISTL1* for adult maize g_c combined from two environments in San Diego, CA, in the WiDiv panel. The $-\log_{10}$ P -value of each haploblock tested in a mixed linear model analysis of g_c is plotted as a short horizontal line against its physical position (B73 RefGen_v4). The length of a short horizontal line corresponds to the size of that haplotype block. The gray vertical bar represents the physical position of *ISTL1*. The top two haploblocks (blocks 65 and 52) that are most associated with g_c are indicated. Polymorphic and monomorphic haploblocks among the evaluated nNILs are colored in blue and red, respectively.

(4-30231047) only 1,219-bp away from the 3'-end of *ISTL1*. The second most strongly associated ($P = 1.41 \times 10^{-5}$) haploblock, Block 52 (Figure 3; Supplemental Table S7), consisted of 10 haplotypes, with the 16 defining SNPs spanning an 8.6-kb region more than 20-kb upstream of *ISTL1*. These findings suggest that the underlying causal variants are located both upstream and downstream of the *ISTL1* gene.

Validation of *ISTL1* haplotype effects with nested NILs

A set of 12 nNILs (Morales et al., 2020) containing the *ISTL1* genomic region from diverse inbreds that are mostly not represented in the WiDiv panel, introgressed into B73 (Supplemental Table S8), were used to validate haplotype effects observed at *ISTL1* in the WiDiv panel. All 12 evaluated nNILs had lower g_c relative to their corresponding donor parent (Figure 4; Supplemental Table S9), which is to be expected given that the recurrent parent, B73, had a comparable or lower g_c than the donor parents. Compared to B73, two NILs with Tzi8 introgressions (Tzi8-B73_NIL_1160 and Tzi8-B73_NIL_1308) and one NIL with an Oh43 introgression (Oh43-B73_NIL_1005) had significantly lower g_c , while four of the donor parents (Ki11, NC350, Oh43, and Tx303) showed significantly higher g_c (Figure 4; Supplemental Table S9).

Of the two most strongly associated haploblocks in the WiDiv panel, only Block 52 (Supplemental Figure S3), the second-ranked haplotype-based association, was polymorphic among the nNILs (Figure 3). This haploblock, consisting of three segregating haplotypes (Supplemental Figure S3), had a significant association ($P < 0.02$) with g_c among nNILs. The haplotype effect of the Tzi8 NILs, which possess

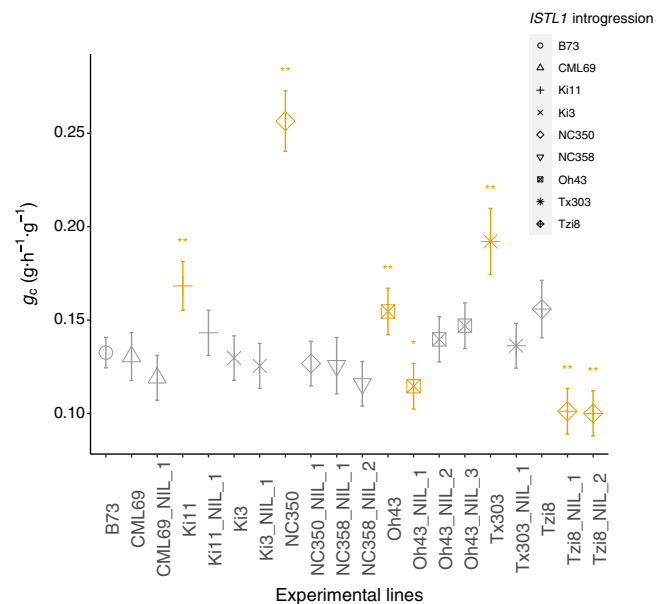


Figure 4 Scatter plot of BLUES for adult maize g_c for B73, nNILs containing *ISTL1* introgressions and their donor parent lines across two environments in San Diego, CA, in 2020. Lines with g_c significantly different from B73 are highlighted in orange. "Asterisk" represents $P < 0.1$ and "Double asterisks" represent $P < 0.05$ after adjustment by the Dunnett's method. Error bars represent standard errors of BLUES.

a unique haplotype relative to B73 and the other donor parents, was significantly ($P = 0.009$ and 0.011) different from the other two haplotypes (Supplemental Figure S3). The Tzi8 haplotype had an effect of $0.1007 \text{ g} \cdot \text{h}^{-1} \cdot \text{g}^{-1}$, whereas the other two haplotypes averaged $\sim 0.13 \text{ g} \cdot \text{h}^{-1} \cdot \text{g}^{-1}$. The smaller effect of the Tzi8 haplotype could explain why both Tzi8 nNILs had the lowest observed g_c values (Figure 4). Haplotype effects of Block 52 strongly correlated ($r = 0.924$) with those estimated in the WiDiv panel (Supplemental Figure S3), indicating that the haplotype effects at *ISTL1* for g_c could be validated in an independent panel having a different population structure.

Discussion

The plant cuticle, as a crucial barrier to water loss (Shepherd and Wynne Griffiths, 2006; Xue et al., 2017), is potentially related to plant drought tolerance (Aharoni et al., 2004; Wang et al., 2012; Zhou et al., 2013; Li et al., 2019). Although major pathways for wax and cutin monomers biosynthesis have been elucidated in model species (Yeats and Rose, 2013; Bakan and Marion, 2017), genetic controls of water loss through leaf cuticles, that is, g_c , remain largely unknown. In a prior study (Lin et al., 2020), we used 235,004 genotyping-by-sequencing (GBS) SNP markers for a GWAS utilizing 451 lines of the WiDiv panel to identify five genomic regions impacting g_c . In this study, we extended this earlier work by imputing genotypes for ~ 9 million SNPs and evaluating the following two features for a subset of 310 WiDiv lines in two growth environments: g_c and

transcript abundances for 20,013 genes in the cuticle maturation zones of developing adult leaf blades. These data were analyzed by GWAS, TWAS, and FCT, greatly increasing the power to identify genes with likely roles in determination of g_c . A total of 22 high-scoring genes (discussed below) from one or more of these tests were identified as plausible candidates based on predicted functions potentially impacting g_c via the regulation of cell wall biosynthesis (2 genes), cuticle biosynthesis and export (4 genes), intracellular membrane trafficking (9 genes), and cuticle development (7 genes) (Figure 2; Table 1). However, regulatory effects are possible for other candidate genes identified in Supplemental Tables S2, Table S4, and Table S5 that were not highlighted as plausible candidates, because their associations with g_c could not be interpreted due to the lack of functional annotations, or predicted functions not readily related to cuticles. Of the 23 GWAS peaks detected in this study, only the GWAS signal associated with *ISTL1* was also found in our previous study that identified five genomic loci associated with g_c (Lin et al., 2020). The main reason for such limited overlap is most likely the extreme difference in the growth environment where associations were found in the prior study (Maricopa, AZ which is very hot and dry) compared to that used for this study (San Diego, CA, which is relatively cool and humid). Subtle changes in population structure when sub-setting the WiDiv population, and different criteria for calling GWAS peaks in this study, may also have contributed to differences in GWAS signals.

Two of the genes identified as plausible candidates for g_c determination have predicted functions in cell wall modification, in particular pectin esterification (PAE5 and PME40). Cutin-embedded polysaccharides present a high degree of esterification, including methylation and acetylation (Philippe et al., 2020). Pectin esterification could be critical to cuticle structure by favoring interactions between cutin and cutin-embedded polysaccharides as well as facilitating the diffusion of cutin precursors (Bakan and Marion, 2017; Philippe et al., 2020) potentially modulating cuticle function as a barrier to water loss.

Our study also pointed to genes encoding predicted cuticle lipid biosynthetic enzymes. FCT identified a maize homolog of CUTIN SYNTHASE1/LI-TOLERANT LIPASE 1, a GDGL acyltransferase that polymerizes cutin precursors extracellularly in Arabidopsis and tomato (Girard et al., 2012; Yeats et al., 2012). FCT and TWAS both identified maize KCS3, a putative component of the fatty acid elongase complex that extends acyl chains produced by the plastid to very long-chain fatty acids. Its closest Arabidopsis relative, KCS2, functions in the two-carbon elongation of acyl chains to C22 very long-chain fatty acyl precursors required for cuticular wax and root suberin biosynthesis (Franke et al., 2009; Lee et al., 2009). Notably, several KCS homologs are upregulated during cuticle maturation in the developing maize adult leaf epidermis (Qiao et al., 2020). TWAS and FCT also identified a maize homolog of *AtCER3* and *ZmGL1*, genes involved in alkane biosynthesis (Sturaro et al., 2005; Bernard et al.,

2012). However, this *GL1*-like/*CER3*-like maize gene has not been previously characterized by forward or reverse genetic approaches. Finally, TWAS analysis identified a maize homolog of Arabidopsis ABCG12/*CER5*, a half-transporter of the ABCG family that forms heterodimers with ABCG11 to transport cuticle lipids across the plasma membrane (Pighin et al., 2004; McFarlane et al., 2010). Unlike the other cuticle biosynthesis candidates highlighted in this study, this maize *CER5* homolog is epidermally upregulated during cuticle maturation (Qiao et al., 2020). Identification of several candidate genes with predicted functions in the biosynthesis and transport of cuticle lipids is consistent with our finding that g_c can be partially predicted by cuticular wax composition.

The biosynthesis of plant cuticles is regulated in a complex network (Yeats and Rose, 2013). In this study, we identified maize homologs of three known regulators of cuticle development (Figure 2; Table 1). This includes a maize homolog of Arabidopsis *CER7*, a core subunit of exosomal 3'-to 5'-exoribonuclease. This enzyme reduces the degradation of *CER3*/*WAX2*/*YORE-YORE* transcripts (Hooker et al., 2007). *CER3* and *CER1* proteins interact to jointly synthesize very-long-chain-alkane (Bernard et al., 2012), an important class of cuticle waxes that is related to drought tolerance (Kosma et al., 2009; Wang et al., 2015, 2020). Interestingly, a different maize *CER7* homolog was associated with g_c in our prior GWAS (Lin et al., 2020), underscoring the potential importance of *CER7* proteins in the regulation of g_c . TWAS identified maize *CER9*, homologous to an Arabidopsis E3 ubiquitin ligase whose deficiency enhances plant drought tolerance via alteration of cuticle composition and reduction of cuticular transpiration (Lü et al., 2012). Finally, both GWAS and FCT identified a maize homolog of Arabidopsis *MIEL1*, an E3 ligase that regulates ABA sensitivity by controlling the protein stability of *MBY96* and *MYB30*, *R2R3-MYB* subfamily regulators of extracellular lipid biosynthesis (Raffaele et al., 2008; Seo et al., 2011), which are important for balanced cuticular wax biosynthesis (Marino et al., 2013; Lee and Seo, 2016; Gil et al., 2017).

Four putative transcriptional regulators of cuticle biosynthesis were also identified as plausible g_c candidates: one *WRKY*, one homeodomain, and two *MYB* transcription factors (Figure 2; Table 1). *WRKY64* has not been directly associated with cuticle development, but a closely related gene in Arabidopsis (*AtWRKY28*; *mybAT4G18170*; Supplemental Table S6) (Jiang et al., 2014) and its maize homolog, *ZmWRKY28* (*Zm00001d011413*), are implicated in cuticle development (Qiao et al., 2020). *MYB108* is homologous to *ATMYB36*, which directly and positively regulates formation of the Casparian strip (characterized by deposition of suberin, which is chemically similar to cutin; Kamiya et al., 2015). *MYB108* is also differentially expressed across the time course of maize leaf cuticular maturation (Qiao et al., 2020). The closest Arabidopsis relative (*AtMYB17*) of FCT-identified *MYB54* (Supplemental Table S6) belongs to the same clade as two well-characterized *MYBs* of cuticle biosynthesis, *MYB106* and *MYB16* (Dubos et al., 2010; Oshima

and Mitsuda, 2013). *GLK35*, identified via TWAS and FCT, is predicted to encode a homeodomain-containing transcription factor that has not been previously studied, but its Arabidopsis homolog (AT2G40260) showed greater than eight-fold change in transcript abundance in response to heat stress (Kant et al., 2008). Therefore, *GLK35* could be a regulator for g_c induced by high temperatures. Together, these candidate genes highlight the potential for developmental and environmental regulation of cuticle formation through transcriptional, posttranscriptional, and posttranslational mechanisms.

Several candidate genes identified in our study have predicted functions in intracellular membrane trafficking, the process by which proteins and lipids are moved from one cellular location to another. These candidates are noteworthy because of prior evidence of a role for membrane trafficking in cuticle formation (McFarlane et al., 2014). Two of our candidate genes encode proteins predicted to function in vesicle formation. One of these is a putative COPI coat component ($\alpha 1$ -COP). COPI has not been widely studied in plants, but COPI deficiency in yeast (*Saccharomyces cerevisiae*) leads to protein accumulation in the endoplasmic reticulum and global secretion deficiency (Lodish et al., 2016). The other is a putative member of SEC14 family phosphatidylinositol transfer protein and is different from the two SEC14 homologs we identified previously as candidate regulators of g_c via GWAS (Lin et al., 2020). Four of our candidate genes have predicted functions in vesicle targeting or fusion, including one putative SNARE, a putative exocyst subunit (SEC15B), and three Rab-GAP domain family proteins with expected functions in regulation of Rab GTPases. By different mechanisms, exocyst, Rab, and SNARE proteins mediate docking and fusion of secretory vesicles, ensuring the specificity of fusion between particular vesicle types and their appropriate target membranes (Saito and Ueda, 2009). These candidate regulators of g_c have potential functions in targeted delivery, to the outer face of epidermal cells, of cuticular lipids as well as proteins such as lipid transporters that are needed for cuticle assembly, thereby impacting the water barrier function of the cuticle.

The final candidate with a predicted membrane trafficking function, *ISTL1*, is of particular interest because it was also identified in our prior GWAS (Lin et al., 2020), and is the only candidate in this study identified by all three approaches: GWAS, TWAS, and FCT. Yeast IST1 promotes the formation of vesicles inside multivesicular bodies (MVBs; Hill and Babst, 2012), a function shared by Arabidopsis *ISTL1* (Buono et al., 2016). The MVB is a late endosomal compartment where plasma membrane-derived proteins are degraded after internalization via endocytosis (Lodish et al., 2016). Recent work has demonstrated that Arabidopsis *ISTL1*, in combination with a functionally related protein LIP5, is needed to maintain an ABCG family transporter at the plasma membrane of anther tapetal cells, and it promotes the accumulation of certain wax components deposited on pollen grains by tapetal cells (Goodman et al., 2021).

Thus, it can be speculated that maize *ISTL1* facilitates the localization of plasma membrane transporters that export cuticle components in maize epidermal cells. Alternatively, cuticular lipids may be delivered extracellularly by fusion of MVBs with the plasma membrane.

The association between g_c and the *ISTL1* genomic region was further verified in a haplotype-based association analysis, which has increased statistical power for detecting marker-trait associations relative to GWAS and can also identify favorable haplotypes for breeding projects. Haplotype-based association tests were performed in both the diversity panel and among nNILs. The strong correlation for haplotype effects for Block 52 in the diversity panel and nNILs confirmed the genetic associations across genetic materials and environments (2018 versus 2020). However, the power of our nNIL analysis to detect genetic effects of haplotype variation in the *ISTL1* region was reduced by several limitations. First, we analyzed only 12 nNILs, which represented all the genetic variation in this collection (Morales et al., 2020) with non-B73 haplotype in the *ISTL1* region. This is a relatively small population for this type of analysis when investigating a locus with a moderate genetic effect for a complex trait. In addition, Block 65, which showed the strongest association with g_c in the diversity panel, was monomorphic among nNILs, so the phenotypic effects of this haploblock could not be investigated in the nNIL analysis. Finally, although there were no common introgressions among selected nNILs besides those containing *ISTL1*, candidate genes identified in GWAS, TWAS, and FCT on other introgressions could reduce the contrasts in g_c caused by different *ISTL1* haplotypes. While these experiments provided modest additional evidence of the impact of haplotype variation at *ISTL1* on g_c , a single gene mutation analysis for g_c and wax profiles using materials created by gene editing, RNA interference, or UniformMu transposon insertions would be ultimately needed to prove the role of this gene in g_c regulation and maize leaf cuticle development.

Conclusions

GWAS, TWAS, and FCT together revealed 22 genes and regulatory factors associated with maize adult leaf g_c . These genes have predicted functions related to the synthesis and function of the cuticle. A candidate causal gene encoding *ISTL1* was associated with g_c by all three tests. Haplotype-based association analysis using maize nNILs containing introgressions of the *ISTL1* genomic region from eight inbred donors into a common background (B73) corroborated marker-trait associations found in WiDiv lines, providing additional evidence of a role for *ISTL1* as a determinant of g_c . The *ISTL1* region haplotypes harbored by Tzi8 were consistently associated with reduced g_c and could be introgressed into adapted maize germplasm to potentially increase drought tolerance via a reduction in nonstomatal transpiration (evaporation across the cuticle).

Materials and methods

Plant materials and experimental design

A set of 323 maize (*Z. mays* L.) inbred lines from the WiDiv panel (Hansey et al., 2011) was planted as a single replicate in a 17×19 incomplete block design at two different times (May and June 2018) in the same field (WiDiv18) at University of California San Diego, San Diego, CA, for evaluation of adult g_c . The set consisted of 89 lines that had been previously shown to have the highest or lowest g_c (extreme g_c lines) in San Diego field experiments (Lin et al., 2020) in addition to 234 lines with restricted flowering time selected for maximal genetic diversity using the CDmean method (Rincen et al., 2012). The field design in both environments was augmented by including Mo17 within each incomplete block. Experimental units were one-row plots of 3.66 m in length having approximately 12 plants with 1.02-m inter-row spacing and a 0.61-m alley.

g_c evaluation and analysis

To inform sampling times for each plot in the WiDiv18 experiment, flowering time (days to anthesis [DTA]) was scored as previously described (Lin et al., 2020). The method of Lin et al. (2020) was used to evaluate g_c on an adult leaf from the primary ear node (or one leaf immediately above/below) of five plants (no fewer than two if five were unavailable) from each plot at flowering. The calculation of adult g_c from unit surface area was as follows:

$$g_c(g \cdot h^{-1} \cdot g^{-1}) = -b/\text{dry weight},$$

where b ($g \cdot h^{-1}$) is the coefficient of the linear regression of leaf wet weight (g) on time (h), and dry weight (g).

For each phenotype (g_c or DTA), a mixed linear model was fitted in ASReml-R version 3.0 (Gilmour et al., 2009) that had grand mean and check as fixed effects and environment, genotype, genotype-by-environment interaction, incomplete block within environment, and column within environment as random effects. Model generated Studentized deleted residuals (Neter et al., 1996) were used to remove significant outliers (Bonferroni $\alpha = 0.05$). The model was refitted for each outlier-screened phenotype to generate variance components to calculate heritability on a line-mean basis according to Lin et al. (2020). An iterative mixed model fitting procedure in ASReml-R version 3.0 was then used to select a best-fit model for each outlier-screened dataset (Supplemental Table S10) to generate a best linear unbiased predictor (BLUP) for g_c and DTA for each line (Supplemental Table S11) following the approach of Lin et al. (2020).

Phenotypic and statistical analysis of extreme g_c lines

Of 57 lines evaluated in the WiDiv18 experiment with highest and lowest g_c scores, we eliminated six classified as flint, popcorn, or tropical, leaving 51 lines mostly having membership in the NSS or SSS subpopulations (Lin et al., 2020). These lines were examined for cuticle structure and

composition. For analysis of guard cell cuticles, adult leaf tissue samples from 2 to 5 plants of each line were fixed, cryo-sectioned, and stained with Fluorol Yellow (FY) to fluorescently label cuticles as described by Matschi et al. (2020). FY-stained cuticles were imaged via superresolution confocal microscopy on a Zeiss LSM 880 Confocal using a Plan-Apochromat 63x/1.4 Oil DIC M27 objective, a 488-nm laser line for excitation, and 495–550-nm band pass emission filter. Zeiss Zen Black software (version 2.3) was used to set laser intensity at 13.7% of maximum, master gain voltage at 700, and digital gain at 1. Zen software was further used to process Z-stacks via superresolution Airyscan methodology (Korobchevskaya et al., 2017). Processed images of 2–16 stomata per plant, cut transversely at the midpoint from base to tip of the stomate, were analyzed using measuring tools in ImageJ. Four guard cell cuticle features were quantified as illustrated in Supplemental Figure S1: bumpiness, cuticular flap length, roundness, and sealability. Roundness was not statistically analyzed because of its very low genetic variation. For the same 51 lines, waxes were extracted from adult leaves (two to five samples per line) by submerging tissue in chloroform for 60 s. Extracted leaf wax samples were evaporated under a gentle stream of nitrogen, and wax samples were analyzed with gas chromatography as described in Bourgault et al. (2020).

Random forest regression models were fit to assess the prediction accuracy of g_c using 62 wax and three cuticle features. The 65 features used in modeling were calculated as an across-environment average of values that had been screened for outliers by Studentized deleted residuals (Supplemental Table S12). Forests were grown with the “cforest” function from the R package “party” version 1.3-7 (Strobl et al., 2007). Five-fold cross-validation was performed 50 times to evaluate the mean predictive accuracy for g_c as described in (Lin et al., 2020). Variable importance measures (Supplemental Table S13) were calculated using the “varimp” function in the “party” package. Parameters used for the number of trees grown ($ntree = 1000$) and predictors sampled ($mtry = 10$) were those that maximized predictive accuracy.

Pearson’s correlation was performed to evaluate linear correlations between g_c and the same 65 features. The significance of correlations ($\alpha = 0.05$) was tested using the function “cor.test” in R version 3.5.1 (R Core Team, 2018).

Construction of genomic datasets for association analyses

Genotypic data

The genotype data processing and imputation approach of Wu et al. (2021) was implemented to generate a SNP marker set in B73 RefGen_v4 coordinates for the WiDiv panel. Briefly, a target SNP set consisting of 159,878 biallelic SNPs scored on 451 WiDiv lines with all heterozygous genotypes set to missing was generated by filtering raw genotypes (exclude singletons and doubletons, call rate $\geq 20\%$, heterozygosity $\leq 10\%$, and index of panmixia ≥ 0.8) of a

955,690 GBS SNP set obtained from Lin et al. (2020). The reference SNP genotype set of Wu et al. (2021), which consisted of 14,613,169 SNPs derived from maize HapMap version 3.2.1 (Bukowski et al., 2018), was imputed based on the target GBS SNP set in the 451WiDiv lines via BEAGLE version 5.0 (Browning et al., 2018). The resultant set of imputed genotypes was filtered to enhance SNP quality for the 310 lines with g_c BLUP values, producing a set of 9,715,072 biallelic SNPs with MAF $\geq 5\%$ and predicted dosage $r^2 \geq 0.80$ for conducting GWAS (Supplemental Data Set 1).

RNA-seq data

Leaf samples for RNA-sequencing (RNA-seq) were collected from plants of the WiDiv18 experiment that had not been destructively sampled for evaluating g_c . In both environments, three plants at a similar stage of development per plot were selected to collect tissue samples between 9 and 11 am PST from the proximal, immature, and actively growing 10%–30% section (developing cuticle) of the total length of the longest unexpanded adult leaf (sheath length < 2 cm). The sampled leaf sections, which were immediately frozen in liquid nitrogen, were from the second, third, or fourth fully adult leaf based on the last leaf with epicuticular wax reported by Hirsch et al. (2014). For each plot, leaf tissue samples from the three plants were ground on dry ice and equally pooled to form a composite of ~ 100 mg tissue sample. All samples were randomized into 96-well plates for RNA extraction with the Direct-zol-96 RNA Kit (Zymo Research, Irvine, CA, USA). Libraries constructed with the Lexogen QuantSeq 3' mRNA-Seq Library Kit FWD (Lexogen, Greenland, NH, USA) were sequenced on an Illumina NextSeq 500 (Illumina, San Diego, CA, USA) at the Genomics Facility of the Cornell Institute of Biotechnology.

Raw 3'-QuantSeq reads were cleaned by trimming Illumina adaptors, the first 12 bases, and polyA tails in accordance with Lexogen recommendations. Cleaned reads were aligned to the B73 RefGen_v4 reference genome (Jiao et al., 2017) using HISAT2 version 2.1.0 (Kim et al., 2019) with $-rna\text{-strandness}$ F and other default parameters. Next, counts were generated in HTSeq version 0.11.2 (Anders et al., 2015) using B73 version AGPv4.42 annotation with $-format=bam$, $-type=gene$, and $-stranded=yes$, followed by normalization of the count data using the DESeq2 rlog function (Love et al., 2014). All genes with a normalized count of less than or equal to zero in all samples were removed.

To verify sample provenance, SNPs were called using the 3'-QuantSeq read alignments and compared to GBS SNPs (Lin et al., 2020). SNPs calls were generated from a pileup file created using SAMTools mpileup with default parameters. The called 3'-QuantSeq SNPs were filtered for quality as previously described in Lin et al. (2020), and they were used to calculate percent identity between each pair of 3'-QuantSeq and GBS samples. With a neighbor-joining tree constructed from a percent identity-based dissimilarity matrix in R version 3.5.1 (R Core Team, 2018), RNAseq samples

(14 in Env1 and 7 in Env2) not clustered with their corresponding GBS samples were excluded. Dataset quality was further improved by removing RNAseq samples (18 in Env1 and 28 in Env2) with < 2 million or > 20 million reads, or an overall alignment rate $< 60\%$. The final dataset consisted of 292 (280 unique lines) samples for Env1 and 305 (288 unique lines) samples for Env2.

A mixed linear model was used to combine transcripts that had nonzero rlog-transformed counts for at least 25% of lines in each environment. To generate BLUPs for the retained 20,018 transcripts, the fitted model was the same as that used for generating phenotypic BLUPs, with the exception that sequencing lane was also included as a random effect. To account for inferred confounders, the probabilistic estimation of expression residuals (PEERs; Stegle et al., 2010) approach was applied to the 310 line \times 20,018 gene matrix of BLUP expression values. The resultant PEER values after extracting 20 learned factors were screened for outliers by Studentized deleted residuals. Transcripts with missing values in over 10% of the population after outlier removal were filtered out, producing a final set of 20,013 transcripts across 310 lines for conducting TWAS (Supplemental Data Set 2).

Association analyses

GWAS

Each of the 9,715,072 SNPs was tested for an association with BLUP values of g_c from the 310 lines with a mixed linear model (Zhang et al., 2010) in the R package GAPIT version 3.0 (Lipka et al., 2012) according to Lin et al. (2020). In brief, the mixed linear model controlled for maturity, population stratification, and unequal relatedness by including DTA BLUPs, principal components (PCs) based on a genotype matrix, and a kinship matrix. The PCs were calculated from the 310 line \times 9,715,072 SNP genotype matrix with the "prcomp" function in R version 3.5.1 (R Core Team, 2018). The same SNP genotype matrix was pruned at a linkage disequilibrium (LD) threshold of $r^2 \leq 0.2$ in PLINK version 1.09_beta5 (Purcell et al., 2007), resulting in a subset of 287,023 SNPs used to construct the kinship matrix based on the centered IBS method (Endelman and Jannink, 2012) in TASSEL version 5.0 (Bradbury et al., 2007). The optimal model for GWAS selected by the Bayesian information criterion (Schwarz, 1978) included only the kinship matrix. The amount of phenotypic variation explained by an SNP was approximated with the likelihood-ratio-based R^2 statistic (R^2_{LR}) of Sun et al. (2010).

TWAS

With BLUP values of g_c from the 310 lines as the response variable, TWAS was performed with PEER values for each of the 20,013 expressed genes by fitting a mixed linear model using the *gwas* function with the P3D function set to FALSE in the R package "rrBLUP" version 4.6 (Endelman, 2011). The optimal model included the same kinship matrix from GWAS.

FCT

The FCT was used to combine GWAS and TWAS results according to [Kremling et al. \(2019\)](#). Briefly, the top 10% of the most associated SNPs (971,508) from GWAS were assigned to the nearest gene. The *P*-values of genes not tested in TWAS were set to 1. For each gene, the paired GWAS and TWAS *P*-values were used to conduct a FCT with the sumlog method in the R package “metap” version 1.4 ([Dewey, 2016](#)).

Candidate gene identification

Given that GWAS, TWAS, and FCT have different statistical power and structure, the rankings of *P*-values for each statistical method were used to identify potential candidate genes following that of [Kremling et al. \(2019\)](#). To identify candidate genes from GWAS results, a set of loci was declared among the top 0.01% of SNPs associated with g_c as described by [Wu et al. \(2021\)](#). The search interval for candidate genes was restricted to ± 200 kb of the peak SNP for each of the declared loci following [Lin et al. \(2020\)](#). The top 1% of genes according to their *P*-values was selected from TWAS and FCT results, resulting in comparable numbers of candidate genes across all three methods.

Haplotype-based association analysis of *ISTL1*

Haploblocks in a ± 200 -kb region encompassing the candidate gene encoding *ISTL1* were constructed using the confidence interval method ([Gabriel et al., 2002](#)) in Haploview version 4.2 ([Barrett et al., 2005](#)). The identified 91 haploblocks ([Supplemental Data Set 3](#)), which were created from an LD pruned ($r^2 > 0.9999$) subset of 726 SNPs, were each tested for an association with g_c by fitting a mixed linear model that included the same GWAS kinship matrix in ASReml-R version 3.0 ([Gilmour et al., 2009](#)). Haplotype effects were estimated for each haploblock, and pairwise comparisons were performed using the *predictPlus.asreml* function.

Evaluation of NILs for *ISTL1*

Experimental field design

To assess haplotype effects of *ISTL1* on g_c variation in a common genetic background, 13 nNILs that contain introgressions harboring *ISTL1* were selected. [Supplemental Figure S4](#) shows that only introgressions containing *ISTL1* are in common among all nNILs. The evaluated nNILs were derived from crosses between eight diverse inbred lines (CML69, Ki11, Ki3, NC350, NC358, Oh43, Tx303, and Tzi8) and the recurrent inbred parent B73 ([Morales et al., 2020](#)). In 2020 at the University of California San Diego, the entire experiment of 13 nNILs and their eight introgression donor parents was planted as a single replicate in a 4×6 incomplete block design on two different dates (June 18 and 28) in the same field. Each incomplete block was augmented by B73. Experimental units for the nNIL20 experiment were the same as those in the WiDiv18 experiment.

Analysis of nNILs and their *ISTL1* haplotypes

The collection and processing of g_c data from the nNIL20 experiment were similar to the procedures used for the WiDiv18 experiment, with the exception that best linear unbiased estimators (BLUEs; [Supplemental Table S9](#)) were calculated. Least-squares means of nNILs and donor lines were compared to B73 with the method of [Dunnett \(1955\)](#) in SAS version 9.4 (SAS institute, 2013).

To validate the observed strong effects of *ISTL1* haploblocks on g_c in the WiDiv panel, the haploblocks most significantly associated with g_c in the WiDiv panel were investigated among 12 of the 13 nNILs that produced plants. With HapMap version 3.2.1 SNP genotypes in B73 RefGen_v4 coordinates ([Bukowski et al., 2018](#)) extracted from *ISTL1* haploblocks, haplotypes for B73 and the donor parents were constructed according to those in the WiDiv panel and projected onto their corresponding nNILs by using information from GBS SNP markers of [Morales et al. \(2020\)](#). The haplotype-based association analysis for g_c was performed as described above, except that the GWAS kinship matrix was not needed to control for genetic background effects among tested nNILs.

Data availability statement

All raw 3'-mRNA-seq data are available from the NCBI Sequence Read Archive under BioProject PRJNA773975. [Supplemental Data Sets 1–3](#) are available at CyVerse (https://datacommons.cyverse.org/browse/iplant/home/shared/GoreLab/dataFromPubs/Lin_LeafCuticleTWAS_2021). Code is available from Github (https://github.com/GoreLab/Maize_leaf_cuticle).

Accession numbers

Maize gene IDs from this article can be found in [Table 1](#) and [Supplemental Table S6](#).

Supplemental data

The following materials are available in the online version of this article.

Supplemental Table S1. Pairwise correlations between traits.

Supplemental Table S2. FCT results for g_c .

Supplemental Table S3. GWAS results for g_c .

Supplemental Table S4. Candidate genes identified through GWAS for g_c .

Supplemental Table S5. TWAS results for g_c .

Supplemental Table S6. Rice and Arabidopsis homologs of 22 plausible candidate genes.

Supplemental Table S7. Haplotype association analysis for g_c .

Supplemental Table S8. Genomic introgressions among nNILs.

Supplemental Table S9. BLUE values of g_c and their differences among nNILs.

Supplemental Table S10. Best fitted mixed linear models.

Supplemental Table S11. BLUP values of g_c and flowering time in WiDiv panel.

Supplemental Table S12. Average values of cuticular waxes and stomatal cuticle features.

Supplemental Table S13. Importance scores for cuticular waxes and stomatal cuticle features.

Supplemental Figure S1. Structural features of adult maize leaf guard cell cuticles.

Supplemental Figure S2. Upset plot of overlapping candidate genes between GWAS, TWAS, and FCT.

Supplemental Figure S3. Haplotype effect analysis in the WiDiv panel and nNILs.

Supplemental Figure S4. Physical positions of introgressions among nNILs.

Supplemental Data Set 1. Genotypes of the WiDiv panel used for GWAS.

Supplemental Data Set 2. Transcript abundances of the WiDiv panel used for TWAS.

Supplemental Data Set 3. Haplotypes of the WiDiv panel for the ISTL1 genomic region.

Acknowledgments

We especially thank Akriti Bhattarai, a BTI intern student, Albert Nguyen, Lesley Saldana De Haro, Alfredo Arriola, Hiep Ha, Jessica Davis, Cameron Garland, Anasilvia Herrera Fuentes, Maria Fernanda Salcedo, and Alondra Deras at UCSD for collecting phenotypic data and tissue samples. We thank Peter Balint-Kurti at USDA-ARS Plant Science Research Unit at NC State University for providing seeds of the maize nNILs. We also thank Elise Withers, a BTI intern student, for preliminary evaluation of an early generation computational pipeline for conducting TWAS.

Funding

This research was supported by the National Science Foundation (IOS1444507).

Conflict of interest statement. The authors declare no conflicts of interest.

References

- Aharoni A, Dixit S, Jetter R, Thoenes E, van Arkel G, Pereira A (2004) The SHINE clade of AP2 domain transcription factors activates wax biosynthesis, alters cuticle properties, and confers drought tolerance when overexpressed in *Arabidopsis*. *Plant Cell* **16**: 2463–2480
- Anders S, Pyl PT, Huber W (2015) HTSeq—a Python framework to work with high-throughput sequencing data. *Bioinformatics* **31**: 166–169
- Bakan B, Marion D (2017) Assembly of the cutin polyester: from cells to extracellular cell walls. *Plants* **6**: 57
- Barrett JC, Fry B, Maller J, Daly MJ (2005) Haploview: analysis and visualization of LD and haplotype maps. *Bioinformatics* **21**: 263–265
- Bernard A, Domergue F, Pascal S, Jetter R, Renne C, Faure J-D, Haslam RP, Napier JA, Lessire R, Joubès J (2012) Reconstitution of plant alkane biosynthesis in yeast demonstrates that *Arabidopsis* ECERIFERUM1 and ECERIFERUM3 are core components of a very-long-chain alkane synthesis complex. *Plant Cell* **24**: 3106–3118
- Bessire M, Borel S, Fabre G, Carraça L, Efremova N, Yephremov A, Cao Y, Jetter R, Jacquat AC, Métraux JP, et al. (2011) A member of the PLEIOTROPIC DRUG RESISTANCE family of ATP binding cassette transporters is required for the formation of a functional cuticle in *Arabidopsis*. *Plant Cell* **23**: 1958–1970
- Bi H, Luang S, Li Y, Bazanova N, Morran S, Song Z, Perera MA, Hrmova M, Borisjuk N, Lopato S (2016) Identification and characterization of wheat drought-responsive MYB transcription factors involved in the regulation of cuticle biosynthesis. *J Exp Bot* **67**: 5363–5380
- Bird D, Beisson F, Brigham A, Shin J, Greer S, Jetter R, Kunst L, Wu X, Yephremov A, Samuels L (2007) Characterization of *Arabidopsis* ABCG11/WBC11, an ATP binding cassette (ABC) transporter that is required for cuticular lipid secretion. *Plant J* **52**: 485–498
- Borisjuk N, Hrmova M, Lopato S (2014) Transcriptional regulation of cuticle biosynthesis. *Biotechnol Adv* **32**: 526–540
- Bourdenx B, Bernard A, Domergue F, Pascal S, Léger A, Roby D, Pervent M, Vile D, Haslam RP, Napier JA, et al. (2011) Overexpression of *Arabidopsis* ECERIFERUM1 promotes wax very-long-chain alkane biosynthesis and influences plant response to biotic and abiotic stresses. *Plant Physiol* **156**: 29–45
- Bourgault R, Matschi S, Vasquez M, Qiao P, Sonntag A, Charlebois C, Mohammadi M, Scanlon MJ, Smith LG, Molina I (2020) Constructing functional cuticles: analysis of relationships between cuticle lipid composition, ultrastructure and water barrier function in developing adult maize leaves. *Ann Bot* **125**: 79–91
- Bradbury PJ, Zhang Z, Kroon DE, Casstevens TM, Ramdoss Y, Buckler ES (2007) TASSEL: software for association mapping of complex traits in diverse samples. *Bioinformatics* **23**: 2633–2635
- Browning BL, Zhou Y, Browning SR (2018) A one-penny imputed genome from next-generation reference panels. *Am J Hum Genet* **103**: 338–348
- Bukowski R, Guo X, Lu Y, Zou C, He B, Rong Z, Wang B, Xu D, Yang B, Xie C, et al. (2018) Construction of the third-generation *Zea mays* haplotype map. *GigaScience* **7**: 1–12
- Buono RA, Paez-Valencia J, Miller ND, Goodman K, Spitzer C, Spalding EP, Otegui MS (2016) Role of SKD1 regulators LIP5 and IST1-LIKE1 in endosomal sorting and plant development. *Plant Physiol* **171**: 251–264
- Busta L, Schmitz E, Kosma DK, Schnable JC, Cahoon EB (2021) A co-opted steroid synthesis gene, maintained in sorghum but not maize, is associated with a divergence in leaf wax chemistry. *Proc Natl Acad Sci USA* **118**: e2022982118
- Chen G, Komatsuda T, Ma JF, Nawrath C, Pourkheirandish M, Tagiri A, Hu YG, Sameri M, Li X, Zhao X, et al. (2011) An ATP-binding cassette subfamily G full transporter is essential for the retention of leaf water in both wild barley and rice. *Proc Natl Acad Sci USA* **108**: 12354–12359
- Chen X, Goodwin SM, Boroff VL, Liu X, Jenks MA (2003) Cloning and characterization of the WAX2 gene of *Arabidopsis* involved in cuticle membrane and wax production. *Plant Cell* **15**: 1170–1185
- Chen YA, Scheller RH (2001) SNARE-mediated membrane fusion. *Nat Rev Mol Cell Biol* **2**: 98–106
- DeBono A, Yeats TH, Rose JKC, Bird D, Jetter R, Kunst L, Samuels L (2009) *Arabidopsis* LTPG is a glycosylphosphatidylinositol-anchored lipid transfer protein required for export of lipids to the plant surface. *Plant Cell* **21**: 1230–1238
- Dewey M (2016) metap: Meta-analysis of significance values. R package version 0.7.
- Dubos C, Stracke R, Grotewold E, Weisshaar B, Martin C, Lepiniec L (2010) MYB transcription factors in *Arabidopsis*. *Trends Plant Sci* **15**: 573–581
- Dunnett CW (1955) A Multiple Comparison Procedure for Comparing Several Treatments with a Control. *J Am Stat Assoc* **50**: 1096–1121
- Elango D, Xue W, Chopra S (2020) Genome wide association mapping of epi-cuticular wax genes in *Sorghum bicolor*. *Physiol Mol Biol Plants* **26**: 1727–1737

- Endelman JB (2011) Ridge regression and other kernels for genomic selection with R package rrBLUP. *Plant Genome* 4: 250–255
- Endelman JB, Jannink JL (2012) Shrinkage estimation of the realized relationship matrix. *G3* 2: 1405–1413
- Febrero A, Fernandez S, Molina-Cano JL, Araus JL (1998) Yield, carbon isotope discrimination, canopy reflectance and cuticular conductance of barley isolines of differing glaucousness. *J Exp Bot* 49: 1575–1581
- Ferguson JN, Fernandes SB, Monier B, Miller ND, Allen D, Dmitrieva A, Schmuker P, Lozano R, Valluru R, Buckler ES, et al. (2021) Machine learning-enabled phenotyping for GWAS and TWAS of WUE traits in 869 field-grown sorghum accessions. *Plant Physiol* 187: 1481–1500
- Fich EA, Segerson NA, Rose JKC (2016) The plant polyester cutin: biosynthesis, structure, and biological roles. *Annu Rev Plant Biol* 67: 207–233
- Franke R, Höfer R, Briesen I, Emsermann M, Efremova N, Yephremov A, Schreiber L (2009) The DAISY gene from *Arabidopsis* encodes a fatty acid elongase condensing enzyme involved in the biosynthesis of aliphatic suberin in roots and the chalazal-micropyle region of seeds. *Plant J* 57: 80–95
- Gabriel SB, Schaffner SF, Nguyen H, Moore JM, Roy J, Blumenstiel B, Higgins J, DeFelice M, Lochner A, Faggart M, et al. (2002) The structure of haplotype blocks in the human genome. *Science* 296: 2225–2229
- Gil HL, Kim J, Chung MS, Joon PS (2017) The MIEL1 E3 ubiquitin ligase negatively regulates cuticular wax biosynthesis in *Arabidopsis* stems. *Plant Cell Physiol* 58: 1249–1259
- Gilmour AR, Gogel BJ, Cullis BR, Thompson R, Butler D, Others (2009) ASReml User Guide Release 3.0. VSN International Ltd, Hemel Hempstead
- Girard AL, Mounet F, Lemaire-Chamley M, Gaillard C, Elmorjani K, Vivancos J, Runavot JL, Quemener B, Petit J, Germain V, et al. (2012) Tomato GDSL1 is required for cutin deposition in the fruit cuticle. *Plant Cell* 24: 3119–3134
- Goodman K, Paez-Valencia J, Pennington J, Sonntag A, Ding X, Lee HN, Ahlquist PG, Molina I, Otegui MS (2021) ESCRT components ISTL1 and LIP5 are required for tapetal function and pollen viability. *Plant Cell* 33: 2850–2868
- Guo J, Xu W, Yu X, Shen H, Li H, Cheng D, Liu A, Liu J, Liu C, Zhao S, et al. (2016) Cuticular wax accumulation is associated with drought tolerance in wheat near-isogenic lines. *Front Plant Sci* 7: 1809
- Guo W, Roth D, Walch-Solimena C, Novick P (1999) The exocyst is an effector for Sec4p, targeting secretory vesicles to sites of exocytosis. *EMBO J* 18: 1071–1080
- Hanse CN, Johnson JM, Sekhon RS, Kaeppler SM, de Leon N (2011) Genetic diversity of a maize association population with restricted phenology. *Crop Sci* 51: 704
- Hen-Avivi S, Savin O, Racovita RC, Lee W-S, Adamski NM, Malitsky S, Almekias-Siegl E, Levy M, Vautrin S, Bergès H, et al. (2016) A metabolic gene cluster in the wheat *W1* and the barley *Cer-cqu* loci determines β -diketone biosynthesis and glaucousness. *Plant Cell* 28: 1440–1460
- Hill CP, Babst M (2012) Structure and function of the membrane deformation AAA ATPase Vps4. *Biochim Biophys Acta* 1823: 172–181
- Hirsch CN, Foerster JM, Johnson JM, Sekhon RS, Muttoni G, Vaillancourt B, Peñagaricano F, Lindquist E, Pedraza MA, Barry K, et al. (2014) Insights into the maize pan-genome and pan-transcriptome. *Plant Cell* 26: 121–135
- Hooker TS, Lam P, Zheng H, Kunst L (2007) A core subunit of the RNA-processing/degrading exosome specifically influences cuticular wax biosynthesis in *Arabidopsis*. *Plant Cell* 19: 904–913
- Hunt L, Amsbury S, Baillie A, Movahedi M, Mitchell A, Afsharinafar M, Swarup K, Denyer T, Hobbs JK, Swarup R, et al. (2017) Formation of the stomatal outer cuticular ledge requires a guard cell wall proline-rich protein. *Plant Physiol* 174: 689–699
- Jiang Y, Duan Y, Yin J, Ye S, Zhu J, Zhang F, Lu W, Fan D, Luo K (2014) Genome-wide identification and characterization of the *Populus* WRKY transcription factor family and analysis of their expression in response to biotic and abiotic stresses. *J Exp Bot* 65: 6629–6644
- Jiao Y, Peluso P, Shi J, Liang T, Stitzer MC, Wang B, Campbell MS, Stein JC, Wei X, Chin CS, et al. (2017) Improved maize reference genome with single-molecule technologies. *Nature* 546: 524–527
- Jouannic N, Lepetit M, Vergnolle C, Cantrel C, Gardies AM, Kader JC, Arondel V (1998) Isolation of a cDNA from *Arabidopsis thaliana* that complements the *sec14* mutant of yeast. *Eur J Biochem* 258: 402–410
- Kamiya T, Borghi M, Wang P, Danku JMC, Kalmbach L, Hosmani PS, Naseer S, Fujiwara T, Geldner N, Salt DE (2015) The MYB36 transcription factor orchestrates Casparian strip formation. *Proc Natl Acad Sci USA* 112: 10533–10538
- Kant P, Gordon M, Kant S, Zolla G, Davydov O, Heimer YM, Chalifa-Caspi V, Shaked R, Barak S (2008) Functional-genomics-based identification of genes that regulate *Arabidopsis* responses to multiple abiotic stresses. *Plant Cell Environ* 31: 697–714
- Kerstiens G (2006) Water transport in plant cuticles: an update. *J Exp Bot* 57: 2493–2499
- Kim D, Paggi JM, Park C, Bennett C, Salzberg SL (2019) Graph-based genome alignment and genotyping with HISAT2 and HISAT-genotype. *Nat Biotechnol* 37: 907–915
- Kim H, Lee SB, Kim HJ, Min MK, Hwang I, Suh MC (2012) Characterization of glycosylphosphatidylinositol-anchored lipid transfer protein 2 (LTPG2) and overlapping function between LTPG/LTPG1 and LTPG2 in cuticular wax export or accumulation in *Arabidopsis thaliana*. *Plant Cell Physiol* 53: 1391–1403
- Korobchevskaya, K, Lagerholm, BC, Colin-York, H, Fritzsche, M (2017) Exploring the potential of airyscan microscopy for live cell imaging. *Photonics* 4: 41
- Kosma DK, Bourdenx B, Bernard A, Parsons EP, Lü S, Joubès J, Jenks MA (2009) The impact of water deficiency on leaf cuticle lipids of *Arabidopsis*. *Plant Physiol* 151: 1918–1929
- Kosma DK, Jenks MA (2007) Eco-physiological and molecular-genetic determinants of plant cuticle function in drought and salt stress tolerance. *Advances in Molecular Breeding Toward Drought and Salt Tolerant Crops*. Springer Science & Business Media, Berlin, Germany, pp 91–120
- Kremling KAG, Diepenbrock CH, Gore MA, Buckler ES, Bandillo NB (2019) Transcriptome-Wide Association Supplements Genome-Wide Association in *Zea mays*. *G3* 9: 3023–3033
- Lee C, Goldberg J (2010) Structure of coatamer cage proteins and the relationship among COPI, COPII, and clathrin vesicle coats. *Cell* 142: 123–132
- Lee HG, Seo PJ (2016) The *Arabidopsis* MIEL1 E3 ligase negatively regulates ABA signalling by promoting protein turnover of MYB96. *Nat Commun* 7: 12525
- Lee SB, Jung SJ, Go YS, Kim HU, Kim JK, Cho HJ, Park OK, Suh MC (2009) Two *Arabidopsis* 3-ketoacyl CoA synthase genes, KCS20 and KCS2/DAISY, are functionally redundant in cuticular wax and root suberin biosynthesis, but differentially controlled by osmotic stress. *Plant J* 60: 462–475
- Lee SB, Suh MC (2015) Advances in the understanding of cuticular waxes in *Arabidopsis thaliana* and crop species. *Plant Cell Rep* 34: 557–572
- Li L, Du Y, He C, Dietrich CR, Li J, Ma X, Wang R, Liu Q, Liu S, Wang G, et al. (2019) Maize *glossy6* is involved in cuticular wax deposition and drought tolerance. *J Exp Bot* 70: 3089–3099
- Lin M, Matschi S, Vasquez M, Chamness J, Kaczmar N, Baseggio M, Miller M, Stewart EL, Qiao P, Scanlon MJ, et al. (2020) Genome-wide association study for maize leaf cuticular conductance identifies candidate genes involved in the regulation of cuticle development. *G3* 10: 1671–1683

- Lipka AE, Tian F, Wang Q, Peiffer J, Li M, Bradbury PJ, Gore MA, Buckler ES, Zhang Z (2012) GAPIT: genome association and prediction integrated tool. *Bioinformatics* **28**: 2397–2399
- Lodish H, Berk A, Kaiser CA, Krieger M, Bretscher A, Ploegh H, Amon A, Martin KC (2016) *Molecular Biology of the Cell*, 8th edn. W.H. Freeman, New York, NY
- Love MI, Huber W, Anders S (2014) Moderated estimation of fold change and dispersion for RNA-seq data with DESeq2. *Genome Biol* **15**: 550
- Lü S, Zhao H, Des Marais DL, Parsons EP, Wen X, Xu X, Bangarusamy DK, Wang G, Rowland O, Juenger T, et al. (2012) *Arabidopsis* ECERIFERUM9 involvement in cuticle formation and maintenance of plant water status. *Plant Physiol* **159**: 930–944
- Marino D, Froidure S, Canonne J, Ben Khaled S, Khafif M, Pouzet C, Jauneau A, Roby D, Rivas S (2013) *Arabidopsis* ubiquitin ligase MIEL1 mediates degradation of the transcription factor MYB30 weakening plant defence. *Nat Commun* **4**: 1476
- Matschi S, Vasquez MF, Bourgault R, Steinbach P, Chamness J, Kaczmar N, Gore MA, Molina I, Smith LG (2020) Structure-function analysis of the maize bulliform cell cuticle and its potential role in dehydration and leaf rolling. *Plant Direct* **4**: e00282
- Mayers JR, Hu T, Wang C, Cárdenas JJ, Tan Y, Pan J, Bednarek SY (2017) SCD1 and SCD2 form a complex that functions with the exocyst and RabE1 in exocytosis and cytokinesis. *Plant Cell* **29**: 2610–2625
- McFarlane HE, Shin JJH, Bird DA, Samuels AL (2010) *Arabidopsis* ABCG transporters, which are required for export of diverse cuticular lipids, dimerize in different combinations. *Plant Cell* **22**: 3066–3075
- McFarlane HE, Watanabe Y, Yang W, Huang Y, Ohlrogge J, Lacey Samuels A (2014) Golgi- and trans-golgi network-mediated vesicle trafficking is required for wax secretion from epidermal cells. *Plant Physiol* **164**: 1250–1260
- Morales L, Repka AC, Swarts KL, Stafstrom WC, He Y, Sermons SM, Yang Q, Lopez-Zuniga LO, Rucker E, Thomason WE, et al. (2020) Genotypic and phenotypic characterization of a large, diverse population of maize near-isogenic lines. *Plant J* **103**: 1246–1255
- Neter J, Kutner MH, Nachtsheim CJ, Wasserman W (1996) *Applied Linear Statistical Models*. Irwin, Chicago, IL
- Oshima Y, Mitsuda N (2013) The MIXTA-like transcription factor MYB16 is a major regulator of cuticle formation in vegetative organs. *Plant Signal Behav* **8**: e26826
- Panikashvili D, Shi JX, Bocobza S, Franke RB, Schreiber L, Aharoni A (2010) The *Arabidopsis* DSO/ABCG11 transporter affects cutin metabolism in reproductive organs and suberin in roots. *Mol Plant* **3**: 563–575
- Patwari P, Salewski V, Gutbrod K, Kreszies T, Dresen-Scholz B, Peisker H, Steiner U, Meyer AJ, Schreiber L, Dörmann P (2019) Surface wax esters contribute to drought tolerance in *Arabidopsis*. *Plant J* **98**: 727–744
- Philippe G, Geneix N, Petit J, Guillon F, Sandt C, Rothan C, Lahaye M, Marion D, Bakan B (2020) Assembly of tomato fruit cuticles: a cross-talk between the cutin polyester and cell wall polysaccharides. *New Phytol* **226**: 809–822
- Pighin JA, Zheng H, Balakshin LJ, Goodman IP, Western TL, Jetter R, Kunst L, Samuels AL (2004) Plant cuticular lipid export requires an ABC transporter. *Science* **306**: 702–704
- Pignon CP, Fernandes SB, Valluru R, Bandillo N, Lozano R, Buckler E, Gore MA, Long SP, Brown PJ, Leahey ADB (2021) Phenotyping stomatal closure by thermal imaging for GWAS and TWAS of water use efficiency-related genes. *Plant Physiol* **187**: 2544–2562
- Pollard M, Beisson F, Li Y, Ohlrogge JB (2008) Building lipid barriers: biosynthesis of cutin and suberin. *Trends Plant Sci* **13**: 236–246
- Purcell S, Neale B, Todd-Brown K, Thomas L, Ferreira MAR, Bender D, Maller J, Sklar P, de Bakker PIW, Daly MJ, et al. (2007) PLINK: a tool set for whole-genome association and population-based linkage analyses. *Am J Hum Genet* **81**: 559–575
- Qiao P, Bourgault R, Mohammadi M, Matschi S, Philippe G, Smith LG, Gore MA, Molina I, Scanlon MJ (2020) Transcriptomic network analyses shed light on the regulation of cuticle development in maize leaves. *Proc Natl Acad Sci USA* **117**: 12464–12471
- R Core Team (2018) R: a language and environment for statistical computing. R Foundation for Statistical Computing, R Core Team, Vienna, Austria.
- Raffaele S, Vaillau F, Léger A, Joubès J, Miersch O, Huard C, Blée E, Mongrand S, Domergue F, Roby D (2008) A MYB transcription factor regulates very-long-chain fatty acid biosynthesis for activation of the hypersensitive cell death response in *Arabidopsis*. *Plant Cell* **20**: 752–767
- Riederer M, Schreiber L (2001) Protecting against water loss: analysis of the barrier properties of plant cuticles. *J Exp Bot* **52**: 2023–2032
- Rincenc R, Laloë D, Nicolas S, Altmann T, Brunel D, Revilla P, Rodriguez VM, Moreno-Gonzalez J, Melchinger A, Bauer E, et al. (2012) Maximizing the reliability of genomic selection by optimizing the calibration set of reference individuals: comparison of methods in two diverse groups of maize inbreds (*Zea mays* L.). *Genetics* **192**: 715–728
- Sadler C, Schroll B, Zeisler V, Waßmann F, Franke R, Schreiber L (2016) Wax and cutin mutants of *Arabidopsis*: quantitative characterization of the cuticular transport barrier in relation to chemical composition. *Biochim Biophys Acta* **1861**: 1336–1344
- Saito C, Ueda T (2009) Chapter 4: functions of RAB and SNARE proteins in plant life. *Int Rev Cell Mol Biol* **274**: 183–233
- Schwarz G (1978) Estimating the dimension of a model. *Ann Stat* **6**: 461–464
- Seo PJ, Lee SB, Suh MC, Park MJ, Go YS, Park CM (2011) The MYB96 transcription factor regulates cuticular wax biosynthesis under drought conditions in *Arabidopsis*. *Plant Cell* **23**: 1138–1152
- Shepherd T, Wynne Griffiths D (2006) The effects of stress on plant cuticular waxes. *New Phytol* **171**: 469–499
- Stegle O, Parts L, Durbin R, Winn J (2010) A Bayesian framework to account for complex non-genetic factors in gene expression levels greatly increases power in eQTL studies. *PLoS Comput Biol* **6**: e1000770
- Stenmark H (2009) Rab GTPases as coordinators of vesicle traffic. *Nat Rev Mol Cell Biol* **10**: 513–525
- Strobl C, Boulesteix AL, Zeileis A, Hothorn T (2007) Bias in random forest variable importance measures: illustrations, sources and a solution. *BMC Bioinformatics* **8**: 25
- Sturaro M, Hartings H, Schmelzer E, Velasco R, Salamini F, Motto M (2005) Cloning and characterization of GLOSSY1, a maize gene involved in cuticle membrane and wax production. *Plant Physiol* **138**: 478–489
- Sun G, Zhu C, Kramer MH, Yang S-S, Song W, Piepho H-P, Yu J (2010) Variation explained in mixed-model association mapping. *Heredity* **105**: 333–340
- Tibbs Cortes L, Zhang Z, Yu J (2021) Status and prospects of genome-wide association studies in plants. *Plant Genome* **14**: e20077
- Valeska Zeisler-Diehl V, Migdal B, Schreiber L (2017) Quantitative characterization of cuticular barrier properties: methods, requirements, and problems. *J Exp Bot* **68**: 5281–5291
- Wang W, Zhang Y, Xu C, Ren J, Liu X, Black K, Gai X, Wang Q, Ren H (2015) Cucumber ECERIFERUM1 (CsCER1), which influences the cuticle properties and drought tolerance of cucumber, plays a key role in VLC alkanes biosynthesis. *Plant Mol Biol* **87**: 219–233
- Wang Y, Jin S, Xu Y, Li S, Zhang S, Yuan Z, Li J, Ni Y (2020) Overexpression of BnKCS1-1, BnKCS1-2, and BnCER1-2 promotes

- cuticular wax production and increases drought tolerance in *Brassica napus*. *Crop J* **8**: 26–37
- Wang Y, Wan L, Zhang L, Zhang Z, Zhang H, Quan R, Zhou S, Huang R** (2012) An ethylene response factor OsWR1 responsive to drought stress transcriptionally activates wax synthesis related genes and increases wax production in rice. *Plant Mol Biol* **78**: 275–288
- Wilmer C, Fricker M** (1996) *Stomata*, 2nd edn. Chapman and Hall, London
- Wu D, Tanaka R, Li X, Ramstein GP, Cu S, Hamilton JP, Buell CR, Stangoulis J, Rocheford T, Gore MA** (2021) High-resolution genome-wide association study pinpoints metal transporter and chelator genes involved in the genetic control of element levels in maize grain. *G3* **11**: jkab059
- Xue D, Zhang X, Lu X, Chen G, Chen Z-H** (2017) Molecular and evolutionary mechanisms of cuticular wax for plant drought tolerance. *Front Plant Sci* **8**: 621
- Yeats TH, Martin LBB, Viart HM-F, Isaacson T, He Y, Zhao L, Matas AJ, Buda GJ, Domozych DS, Clausen MH, et al.** (2012) The identification of cutin synthase: formation of the plant polyester cutin. *Nat Chem Biol* **8**: 609–611
- Yeats TH, Rose JKC** (2013) The formation and function of plant cuticles. *Plant Physiol* **163**: 5–20
- Zhang JY, Broeckling CD, Blancaflor EB, Sledge MK, Sumner LW, Wang ZY** (2005) Overexpression of WXP1, a putative *Medicago truncatula* AP2 domain-containing transcription factor gene, increases cuticular wax accumulation and enhances drought tolerance in transgenic alfalfa (*Medicago sativa*). *Plant J* **42**: 689–707
- Zhang Z, Ersoz E, Lai CQ, Todhunter RJ, Tiwari HK, Gore MA, Bradbury PJ, Yu J, Arnett DK, Ordovas JM, et al.** (2010) Mixed linear model approach adapted for genome-wide association studies. *Nat Genet* **42**: 355–360
- Zhao L, Sack FD** (1999) Ultrastructure of stomatal development in *Arabidopsis* (Brassicaceae) leaves. *Am J Bot* **86**: 929–939
- Zhou L, Ni E, Yang J, Zhou H, Liang H, Li J, Jiang D, Wang Z, Liu Z, Zhuang C** (2013) Rice *OsGL1-6* is involved in leaf cuticular wax accumulation and drought resistance. *PLoS One* **8**: e65139
- Zhu X, Xiong L** (2013) Putative megaenzyme DWA1 plays essential roles in drought resistance by regulating stress-induced wax deposition in rice. *Proc Natl Acad Sci USA* **110**: 17790–17795